World Academy of Science, Engineering and Technology
International Journal of Aerospace and Mechanical Engineering
Vol:12, No:3, 2018

Nonlinear Modelling of Sloshing Waves and Solitary Waves in Shallow Basins

Mohammad R. Jalali, Mohammad M. Jalali

Open Science Index, Aerospace and Mechanical Engineering Vol:12, No:3, 2018 publications.waset.org/10008925/pdf

***Abstract*—**The earliest theories of sloshing waves and solitary waves based on potential theory idealisations and irrotational flow have been extended to be applicable to more realistic domains. To this end, the computational fluid dynamics (CFD) methods are widely used. Three-dimensional CFD methods such as Navier-Stokes solvers with volume of fluid treatment of the free surface and Navier-Stokes solvers with mappings of the free surface inherently impose high computational expense; therefore, considerable effort has gone into developing depth-averaged approaches. Examples of such approaches include Green–Naghdi (GN) equations. In Cartesian system, GN velocity profile depends on horizontal directions, x-direction and y-direction. The effect of vertical direction (z-direction) is also taken into consideration by applying weighting function in approximation. GN theory considers the effect of vertical acceleration and the consequent non-hydrostatic pressure. Moreover, in GN theory, the flow is rotational. The present study illustrates the application of GN equations to propagation of sloshing waves and solitary waves. For this purpose, GN equations solver is verified for the benchmark tests of Gaussian hump sloshing and solitary wave propagation in shallow basins. Analysis of the free surface sloshing of even harmonic components of an initial Gaussian hump demonstrates that the GN model gives predictions in satisfactory agreement with the linear analytical solutions. Discrepancies between the GN predictions and the linear analytical solutions arise from the effect of wave nonlinearities arising from the wave amplitude itself and wave-wave interactions. Numerically predicted solitary wave propagation indicates that the GN model produces simulations in good agreement with the analytical solution of the linearised wave theory. Comparison between the GN model numerical prediction and the result from perturbation analysis confirms that nonlinear interaction between solitary wave and a solid wall is satisfactorilly modelled. Moreover, solitary wave propagation at an angle to the x-axis and the interaction of solitary waves with each other are conducted to validate the developed model.

***Keywords*—**Even harmonic components of sloshing waves, Green–Naghdi equations, nonlinearity, solitary waves.

I. Introduction

FREE surface waves can be categorised as progressive, sloshing, and solitary waves of displacement depending on whether they are excited as free or forced surface responses in a container, or shear driven waves in an open domain, or displaced waves. The movement of liquid with a free surface in a container is known as slosh. For instance, slosh occurs when water in a closed tank is set in motion by a free surface displacement, or when liquid natural gas in a container is vibrated by an external driving force such as earthquake or movement induced by transport. According to [1], sloshing theories originate from fluid field equations for behaviour of free surface waves whereby linearised mass and momentum equations are applied as governing equations. The linearised solution of sloshing behaviour is not exactly realistic since not only does the position of free surface vary, but also the combined free surface boundary condition is nonlinear, involving mixed kinematic and dynamic boundary conditions. The nonlinear behaviour of sloshing is particularly affected by the initial wave amplitude (which is assumed to be zero in linear models). Slosh motions can be categorised as simple planar, rotational, symmetric, asymmetric, and chaotic [1].

Solitary waves propagate along the channel without any change in their form, elevation and velocity. In 1834 John Scott Russell was the first person to discover this type of wave when he observed a solitary-type wave released by a boat as it manoeuvred in the Union Canal at Hermiston. Scott Russell reported that: the wave speed is dependent on the ratios of wave amplitude and wave width with respect to the water depth; and interaction of solitary waves with each other does not change their original features [2]. Waves in the open ocean and in liquid containers and basins are often approximated by infinite Fourier series of sine and cosine waves which are dispersive and may travel in different directions depending on the mode of generation [3]. This linear representation of ocean sea states ignores inherently nonlinear pre-breaking wave behaviour (peaked crests and broad troughs) and nonlinear wave-wave interactions. To extend to more realistic domains, the three-dimensional (3D) computational methods have become widely used. The 3D computational methods undergo inherently high computational expense; therefore, considerable effort has gone into depth-averaged approaches, they being cheaper to compute and yet capturing much of the physics. Green and Naghdi [4] proposed a theory of fluid sheets known as GN theory to model the two-dimensional (2D) continuum of unsteady inviscid 3D flows. According to [5], the GN approach assumes a particular flow kinematic structure in the vertical direction for shallow and deep water problems. In GN theory, the fluid velocity profile is a finite sum of coefficients depending on space and time multiplied by a weighting function. GN theory is not based on priori assumptions on any scaling parameter or perturbation expansion. GN fluid sheet theory reduces the dimensions from three to two, yielding equations that can be solved efficiently so that no scale is introduced and no term is deleted [5]. Reference [6] derived the k^{th} level theory of GN equations. In the present study, GN equations are applied to simulate the nonlinear behaviour of sloshing waves.

Mohammad R. Jalali (PhD) and Mohammad M. Jalali (PhD) were with University of Edinburgh, Edinburgh, UK. They are now with School of Mathematics and Statistics, Mathematical institute, University of St Andrews, St Andrews, UK (e-mail: mrj3@st-andrews.ac.uk, mmj5@st-andrews.ac.uk).

Open Science Index, Aerospace and Mechanical Engineering Vol:12, No:3, 2018 publications.waset.org/10008925/pdf

An analytic solitary wave solution of the level I GN equations is presented by [7] for solitary wave generation through moving disturbance in shallow water. Reference [8] examined the convergence of the solitary wave and periodic wave solutions of the first three levels of the GN equations. Reference [8] concluded that the best convergence was related to higher levels of theory for critical speed. Reference [9] developed an irrotational Green-Naghdi (IGN) model of large-amplitude nonlinear wave propagation and irregular wave-wave interactions in deep water. Reference [10] proposed a hybrid numerical method employing a Godunov-type scheme to solve the GN model for dispersive shallow water waves in transcritical flows, including dam-breaks. Reference [11] examined the applicability of level I GN equations to solitary wave propagation over a gradually changing bathymetry. In these studies, good agreement was obtained between the laboratory data and level I GN predictions. Reference [12] studied nonlinear solitary waves in constant and variable water depths by applying original level I GN equations and different levels of IGN equations. Reference [12] verified their models through various tests such as: (1) Solitary wave propagating from deep water to shallow water (and vice versa), with a linear transition between the two depths. (2) Solitary wave propagating over a submerged curved bump. (3) Reflection of a solitary wave from a vertical wall. (4) Interaction (collision and overtaking) of two solitary waves over a flat seafloor. (5) Waves produced by an initial mound of water (dam break problem). In all the solitary wave cases, it was concluded that with increase of nonlinearity, level I GN equations compared to higher levels of IGN equations underestimates higher harmonics. Reference [13] used Newton–Raphson method to develop steady-state solitary wave solution of high-level GN equations, in which different solitary wave features such as wave speed, wave profile and velocity field were examined.

In the present study, a numerical model is developed to simulate nonlinear even harmonic oscillations of free surface sloshing of an initial Gaussian hump in basin. For this purpose, 2D level I GN equations are applied as governing equations of fluid field to produce nonlinear second-order and higher-order wave interactions. Moreover, the solitary wave propagation in wall-banded basin is examined by applying level I GN numerical solver. In another test, level I GN numerical solver is used to simulate the nonlinear interaction of two solitary waves with solid wall and their interaction with each other. Sections II and III present the derivation of governing GN equations. Sections IV and V outline the numerical implementation. Sections VI and VII, respectively, demonstrate the results for free surface sloshing of even harmonic components of an initial Gaussian hump and solitary wave propagation in basins. Section VIII presents the result for interaction of two solitary waves in wall-bounded basin. Section IX is the summary of the main findings.

II. Continuity Equation of Level I GN Equations

The classical mass conservation equation is applied to drive GN continuity equation:

$$\frac{\partial u}{\partial x}+\frac{\partial v}{\partial y}+\frac{\partial w}{\partial z}=0 \tag{1}$$

in which u, v, w are the velocity components in the x, y, z directions. In order to derive the GN continuity equation, the velocity vector ($\boldsymbol{V}$) is written as follows:

$$\boldsymbol{V}=\sum_{n=0}^{e}\overrightarrow{W_n}(x,y,t)\,\lambda_n(z) \tag{2}$$

Here, $\overrightarrow{W_n}=(u_n,v_n,w_n)$ is a vector of velocity component approximations, λ_n is assumed shape functions which depends on z-direction, and e is the level of approximation of GN theory. GN velocity parameters for level I are:

$$\begin{aligned} u(x,y,z,t)&=u_0(x,y,t)\\ v(x,y,z,t)&=v_0(x,y,t)\\ w(x,y,z,t)&=w_0(x,y,t)+w_1(x,y,t)(z)\end{aligned} \tag{3}$$

in which $\lambda_0(z)=1$, $\lambda_1(z)=z$, $u_1(x,y,t)=v_1(x,y,t)=0$. w_1 and w_0 in (3) are:

$$w_1=-\left(\frac{\partial u_0}{\partial x}+\frac{\partial v_0}{\partial y}\right),\quad w_0=0 \tag{4}$$

More details on above assumptions are provided by [6]. By applying (3) in (1) the 2D level I GN continuity equation is derived:

$$\frac{\partial h}{\partial t}+\frac{\partial u_0 h}{\partial x}+\frac{\partial v_0 h}{\partial y}=0 \tag{5}$$

Here, h is the total water elevation, (u_0, v_0) are the horizontal velocity components, and t is the time. In the present derivation of GN equations, the total water elevation (h) is $h=h_0+\zeta$. Here, h_0 is the still water depth and ζ is the free surface elevation above still water level.

III. Momentum Equations of Level I GN Equations

The classical x-momentum conservation equation is used to drive GN x-momentum equation:

$$\frac{\partial \rho u}{\partial t}+\frac{\partial \rho uu}{\partial x}+\frac{\partial \rho uv}{\partial y}+\frac{\partial \rho uw}{\partial z}=-\frac{\partial P}{\partial x} \tag{6}$$

Here, ρ is water density and P is pressure. Applying depth integration to (6), then using the chain rule for fourth term, and applying Leibnitz Rule for right hand side term yields:

$$\int_0^z \frac{\partial \rho u}{\partial t}\lambda_n\,dz+\int_0^z \frac{\partial \rho uu}{\partial x}\lambda_n\,dz+\int_0^z \frac{\partial \rho uv}{\partial y}\lambda_n\,dz+\rho uw\lambda_n\Big|_0^z$$

Open Science Index, Aerospace and Mechanical Engineering Vol:12, No:3, 2018 publications.waset.org/10008925/pdf

$$-\int_0^z \rho u w \lambda_n' \, dz = -\frac{\partial P_n}{\partial x} + \hat{P}\frac{\partial h}{\partial x}\lambda_n \,|_z \tag{7}$$

where $P_n = \dfrac{\partial\left(\int_0^z P\lambda_n \, dz\right)}{\partial x}$ and $\hat{P}$ is pressure at the free surface (here $\hat{P} = 0$). By applying (2) in (7), the constrained *x*-direction momentum equation of GN equations is:

$$\sum_{r=0}^{e=1}\rho\frac{\partial u_m}{\partial t}y_{mn} + \sum_{m=0}^{e=1}\sum_{r=0}^{e=1}\frac{\partial u_m}{\partial x}u_r\, y_{mrn} + \sum_{m=0}^{e=1}\sum_{r=0}^{e=1}\frac{\partial u_m}{\partial y}v_r\, y_{mrn} + \sum_{m=0}^{e=1}\sum_{r=0}^{e=1}\rho u_m w_r\, y_{nr}^m = -\frac{\partial P_n}{\partial x} \tag{8}$$

where

$$y_{mn} = \int_0^z \lambda_m\lambda_n \, dz\,,\ y_{mrn} = \int_0^z \lambda_m\lambda_r\lambda_n \, dz\,, \text{ and } y_{mr}^n = \int_0^z \lambda_m\lambda_r\lambda_n' \, dz$$

More details are provided by [2], [14].

The constrained *z*-momentum equation of GN equations is:

$$\sum_{r=0}^{e=1}\rho\frac{\partial w_m}{\partial t}y_{mn} + \sum_{m=0}^{e=1}\sum_{r=0}^{e=1}\frac{\partial w_m}{\partial x}u_r\, y_{mrn} + \sum_{m=0}^{e=1}\sum_{r=0}^{e=1}\frac{\partial w_m}{\partial y}v_r\, y_{mrn} + \sum_{m=0}^{e=1}\sum_{r=0}^{e=1}\rho w_m w_r\, y_{rn}^m = P_n' - \rho \boldsymbol{g} y_n \tag{9}$$

in which $P_n' = \int_0^z P\lambda_n' \, dz$ and $\boldsymbol{g}$ is the gravitational acceleration.

By simplifying (8), the 2D level I *x*-momentum GN equation for flat bathymetry is:

$$h\frac{\partial h}{\partial x}\left[-\frac{\partial^2 u_0}{\partial x\partial t} - \frac{\partial^2 v_0}{\partial y\partial t} - u_0\frac{\partial^2 u_0}{\partial x^2} - v_0\frac{\partial^2 v_0}{\partial y^2} - \frac{\partial^2 u_0 v_0}{\partial x\partial y} + \left(\frac{\partial u_0}{\partial x} + \frac{\partial v_0}{\partial y}\right)^2\right] + \boldsymbol{g}\frac{\partial h}{\partial x} + \frac{h^2}{3}\left[-\frac{\partial^3 u_0}{\partial x^2\partial t} - \frac{\partial^3 v_0}{\partial x\partial y\partial t} - u_0\frac{\partial^3 u_0}{\partial x^3} - \frac{\partial^3 u_0 v_0}{\partial x^2\partial y} - v_0\frac{\partial^3 v_0}{\partial x\partial y^2} - \frac{\partial v_0}{\partial x}\left(\frac{\partial^2 u_0}{\partial x\partial y} + \frac{\partial^2 v_0}{\partial y^2}\right) + \left(\frac{\partial u_0}{\partial x} + 2\frac{\partial v_0}{\partial y}\right)\left(\frac{\partial^2 v_0}{\partial x\partial y} + \frac{\partial^2 u_0}{\partial x^2}\right)\right] + \left(\frac{\partial u_0}{\partial t} + u_0\frac{\partial u_0}{\partial x} + v_0\frac{\partial u_0}{\partial y}\right) = 0 \tag{10}$$

Derivation of the 2D level I *y*-momentum GN equation is presented by [2].

IV. Numerical Implementation

According to [15], GN equations (5) and (10) are discretised numerically through second-order central differences as numerical scheme. Continuity equation of GN equations (5) is simply discretised using explicit finite differences. However, GN momentum equations include cross-derivatives (i.e., space derivative and time derivative) terms which cannot be discretised by explicit finite differences. Therefore, implicit tridiagonal matrix inversion is applied to solve the GN momentum equations. The explicitly discretised GN continuity equation (5) is:

$$\frac{\partial h}{\partial t}\Big|_{ij}^t = \left[\left(\frac{u_{0i+1j}^t\, h_{i+1j}^t - u_{0i-1j}^t\, h_{i-1j}^t}{2\Delta x}\right) + \left(\frac{v_{0ij+1}^t\, h_{ij+1}^t - v_{0ij-1}^t\, h_{ij-1}^t}{2\Delta y}\right)\right] \tag{11}$$

Here, *i* refers to *x*-direction, *j* is *y*-direction and *t* is time. The cross-derivatives terms of the GN momentum equation (10) are separated from the rest of space derivative terms

$$\underset{L}{\boldsymbol{F}} = \frac{\partial u_0}{\partial t} - h\frac{\partial h}{\partial x}\frac{\partial}{\partial x}\left(\frac{\partial u_0}{\partial t}\right) - \frac{h^2}{3}\frac{\partial^2}{\partial x^2}\left(\frac{\partial u_0}{\partial t}\right) \tag{12}$$

Equation (12) is discretised by applying second-order finite differences

$$\underset{L}{\boldsymbol{F}}\Big|_{ij}^t = \left[h_{ij}^t\left(\frac{h_{i+1j}^t - h_{i-1j}^t}{4\Delta x^2}\right) - \frac{\left(h_{ij}^t\right)^2}{3\Delta x^2}\right]\tilde{u}_{0i-1j}^t + \left[1 + \frac{2\left(h_{ij}^t\right)^2}{3\Delta x^2}\right]\tilde{u}_{0ij}^t + \left[-h_{ij}^t\left(\frac{h_{i+1j}^t - h_{i-1j}^t}{4\Delta x^2}\right) - \frac{\left(h_{ij}^t\right)^2}{3\Delta x^2}\right]\tilde{u}_{0i+1j}^t \tag{13}$$

In (13) $\tilde{u}_{0ij}^t = \dfrac{\partial u_0}{\partial t}\Big|_{ij}^t$.

Equation (13) can be written in form of matrix coefficients

$$\underset{L}{\boldsymbol{F}}_{ij}^t = \tilde{a}_{ij}^t\,\hat{u}_{0i-1j}^t + \tilde{b}_{ij}^t\,\hat{u}_{0ij}^t + \tilde{c}_{ij}^t\,\hat{u}_{0i+1j}^t \tag{14}$$

Here, $\tilde{a}_{ij}^t$ is the subdiagonal of the matrix solver, $\tilde{b}_{ij}^t$ is the main diagonal of the matrix solver, and c_{ij}^t is the superdiagonal of the matrix solver. Other space derivative terms of (10) are also discretised:

$$\underset{R}{F}\Big|_{ij}^t = -\left[u_{0ij}^t\frac{\partial u_0}{\partial x}\Big|_{ij}^t + v_{0ij}^t\frac{\partial u_0}{\partial y}\Big|_{ij}^t + \boldsymbol{g}\frac{\partial h}{\partial x}\Big|_{ij}^t\right] + \frac{\left(h_{ij}^t\right)^2}{3}\frac{\partial^2}{\partial x\partial y}\left(\frac{\partial v_0}{\partial t}\right)\Big|_{ij}^t + \frac{\left(h_{ij}^t\right)^2}{3}\left[u_{0ij}^t\frac{\partial^3 u_0}{\partial x^3}\Big|_{ij}^t + \frac{\partial^3 u_0 v_0}{\partial x^2\partial y}\Big|_{ij}^t + \frac{\partial v_0}{\partial x}\Big|_{ij}^t\left(\frac{\partial^2 u_0}{\partial x\partial y}\Big|_{ij}^t + \frac{\partial^2 v_0}{\partial y^2}\Big|_{ij}^t\right) + v_{0ij}^t\frac{\partial^3 v_0}{\partial x\partial y^2}\Big|_{ij}^t - \left(\frac{\partial u_0}{\partial x}\Big|_{ij}^t + 2\frac{\partial v_0}{\partial y}\Big|_{ij}^t\right)\left(\frac{\partial^2 v_0}{\partial x\partial y}\Big|_{ij}^t + \frac{\partial^2 u_0}{\partial x^2}\Big|_{ij}^t\right)\right] + h_{ij}^t\frac{\partial h}{\partial x}\Big|_{ij}^t\left[u_{0ij}^t\frac{\partial^2 u_0}{\partial x^2}\Big|_{ij}^t + v_{0ij}^t\frac{\partial^2 v_0}{\partial y^2}\Big|_{ij}^t + \frac{\partial^2 u_0 v_0}{\partial x\partial y}\Big|_{ij}^t - \left(\frac{\partial u_0}{\partial x}\Big|_{ij}^t + \frac{\partial v_0}{\partial y}\Big|_{ij}^t\right)^2\right] + h_{ij}^t\frac{\partial h}{\partial x}\Big|_{ij}^t\frac{\partial}{\partial y}\left(\frac{\partial v_0}{\partial t}\right)\Big|_{ij}^t \tag{15}$$

Open Science Index, Aerospace and Mechanical Engineering Vol:12, No:3, 2018 publications.waset.org/10008925/pdf

Equations (14) and (15) together formed the developed numerical solver for GN momentum equation (10). Thomas algorithm [16] is applied to obtain $\tilde{u}_{0ij}^{t}$.

y-momentum equation is also discretised and the details are presented by [2]. To update the values of water elevation (h) and the velocity profile (u,v), the Runge-Kutta fourth-order (RK4) time-stepping scheme is applied to the GN numerical solver.

V. The Numerical Convergence Examinations

The following benchmark tests are designed: free surface sloshing of even harmonic components of an initial Gaussian hump in a basin and solitary wave propagation in a wall-bounded basin.

To determine the length and width of grids, convergence examinations were carried out for free surface sloshing of even harmonic components of an initial Gaussian hump. To this end, the free surface elevation patterns in the basin of 7.5 m length and 7.5 m width were obtained on increasingly grid size with $\Delta x = \Delta y = 150$ mm (coarse grids), $\Delta x = \Delta y = 37.5$ mm (medium grids), and $\Delta x = \Delta y = 7.5$ mm (fine grids). The medium grid size $\Delta x = \Delta y = 37.5$ mm was sufficient to convergence. Therefore, $\Delta x = \Delta y = 37.5$ mm was chosen for numerical simulations of sloshing of even harmonic components of an initial Gaussian hump. Also, small time-step ($\Delta t = 0.05$ s) was used for numerical predictions of sloshing of even harmonic components of an initial Gaussian hump.

To simulate the solitary wave, 3D visualisations of free surface elevation patterns in a basin of 25 m length and 25 m width were produced on increasingly grid size with $\Delta x = \Delta y = 500$ mm (coarse grids), $\Delta x = \Delta y = 100$ mm (medium grids), and $\Delta x = \Delta y = 50$ mm (fine grids). The medium grid size $\Delta x = \Delta y = 100$ mm was sufficient to convergence. Therefore, $\Delta x = \Delta y = 100$ mm was chosen for numerical simulations of solitary wave propagation. The numerical predictions of free surface profiles of solitary wave for different time steps ($\Delta t = 0.05$, 0.,1 and 0.2 s) revealed that $\Delta t = 0.05$ s was sufficient for producing accurate simulations.

VI. Free Surface Sloshing of Even Harmonic Components of an Initial Gaussian Hump in a Square Flat-Basin

The numerical solver of the 2D level I GN equations is verified for nonlinear free surface sloshing motions arising from the even harmonic components of an initial Gaussian hump and an initial Gaussian trough. According to [17], [18], the even harmonics components are obtained by simulating the free surface time series resulting from releasing the initial hump, and the corresponding free surface time histories produced by an initial trough of equal but opposite shape to the hump. The free surface elevation of Gaussian hump, ζ_c, is:

$$\zeta_c(x,y) = a\exp\left\{-b\left[\left(x-\frac{L_x}{2}\right)^2+\left(y-\frac{L_y}{2}\right)^2\right]\right\} \quad (16)$$

where a is the wave amplitude; b is spreading parameter; and L_x and L_y are the length and width of the basin. The free surface elevation of Gaussian trough, ζ_t, is:

$$\zeta_t(x,y) = -a\exp\left\{-b\left[\left(x-\frac{L_x}{2}\right)^2+\left(y-\frac{L_y}{2}\right)^2\right]\right\} \quad (17)$$

The even harmonics are obtained by additions $\left(\frac{\zeta_c+\zeta_t}{2}\right)$.

A basin of 7.5 m length and 7.5 m width is selected in which the constant water depth is $h_0 = 0.45$ m. The initial amplitude of the hump and trough, a, is 0.225 m and the spreading parameter $b = 2$ m^{-2}.

Figs. 1 and 2, respectively, present the analytical and numerical predictions of free surface elevation time history of the initial Gaussian hump, Gaussian trough and even harmonics components at the centre of basin for a total simulation time of 40 s. As it is observed in Fig. 1, the analytical solution is not capable to show the nonlinear behaviour of even harmonics. However, in Fig. 2, it is possible to see evidence of the nonlinear effect produced by even harmonics. Moreover, Fig. 2 reveals that the even harmonics have amplitudes of up to about 20% that of the initial hump. The foregoing discrepancies in Figs. 1 and 2 are largely due to nonlinear (second-order and higher-order) wave interactions. The nonlinearity of wave interactions is adequately modelled by the 2D level I GN equations, while it is totally neglected in the analytical solution.

To understand better the resonant free surface motions driven by an initial Gaussian disturbance, it is useful to carry out spectral analysis using a Fast Fourier Transform (FFT) of the free surface elevation time series. The FFT reveals the variance of the signal within a given frequency. Each FFT plot includes a series of magnitude peaks, each associated with a particular frequency.

Fig. 3 presents comparison of analytically predicted FFT spectrum for the free surface elevation time history of the initial Gaussian hump, numerically predicted FFT spectrum for the free surface elevation time history of the initial Gaussian hump and numerically predicted FFT spectrum for the free surface elevation time history of even harmonics components at the centre of basin. It can be observed that all five peaks of numerical Gaussian hump occur at the same frequency of the analytically predicted peaks of Gaussian hump. Also, all five peaks of numerical even harmonics occur at the same frequency of the analytically predicted peaks of Gaussian hump.

Fig. 4 shows the even harmonic free surface profiles along the basin at times $t = 0.5$ s and 1 s for analytical and numerical simulations. In Figs. 4 (a) and (b), the analytical solution is not

capable of showing the nonlinear behaviour of even harmonics while, the effect of nonlinearity is evident in numerical simulations in Figs. 4 (c) and (d), as can be seen by the wave motions in the even harmonics.

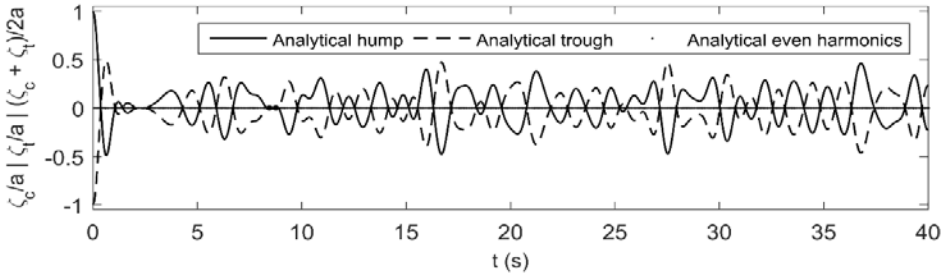


Fig. 1 Analytically predicted free surface elevation time histories at the centre of a basin for sloshing of an initial Gaussian hump (solid line), Gaussian trough (dash line) and even harmonics (cross symbols)

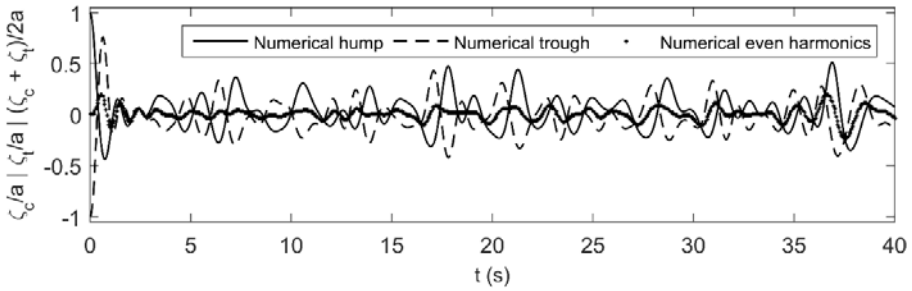


Fig. 2 Numerically predicted free surface elevation time histories at the centre of a basin for sloshing of an initial Gaussian hump (solid line), Gaussian trough (dash line) and even harmonics (cross symbols)

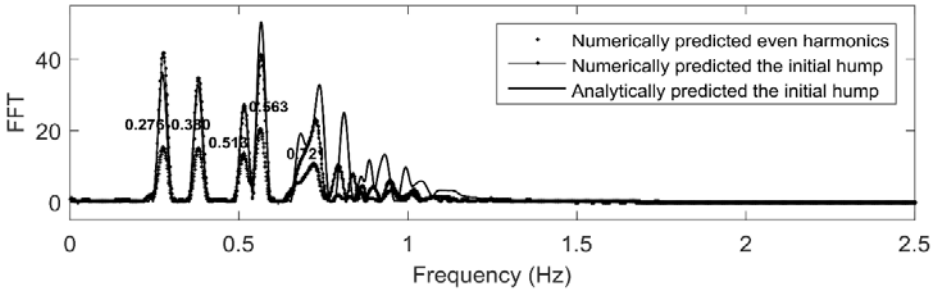
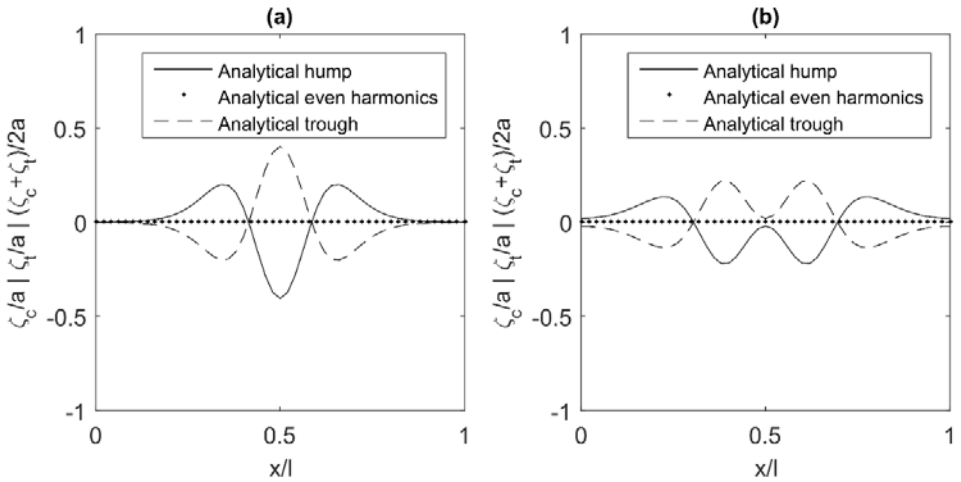


Fig. 3 Comparison of analytical FFT spectrum (solid line) and numerical FFT spectrum (diamond line) of the free surface elevation time history of the initial Gaussian hump with the numerically predicted FFT spectrum of even harmonics (cross symbols)



Open Science Index, Aerospace and Mechanical Engineering Vol:12, No:3, 2018 publications.waset.org/10008925/pdf

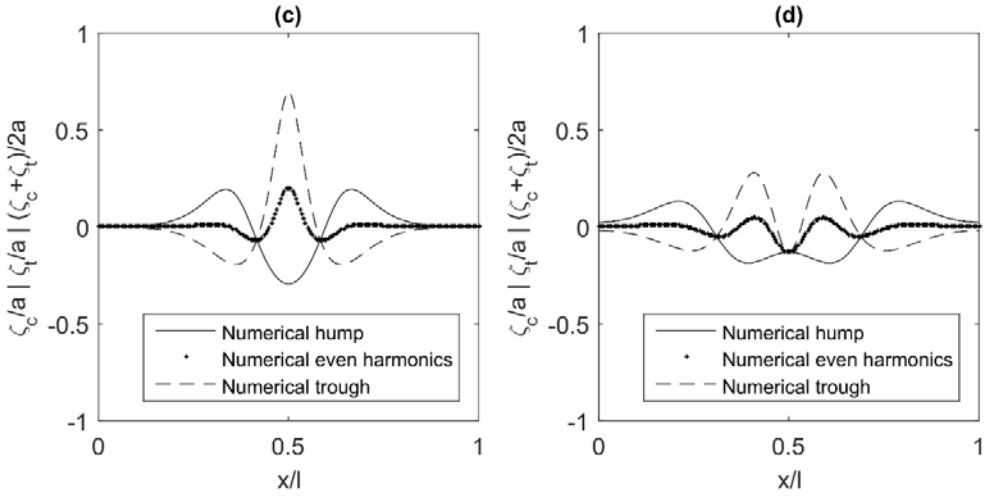


Fig. 4 Initial Gaussian hump (solid line), Gaussian trough (dash line) and even harmonics (cross symbols) profiles along the centerline of the basin: (a) and (b) analytically predicted profiles at t = 0.5 s and 1 s. (c), and (d) numerically predicted profiles at t = 0.5 s and 1 s

VII. Solitary Wave Propagation in Wall-Bounded Basin

The free surface profile of the solitary wave is given by [10]

$$\zeta(x,y,t) = a\ \mathrm{sech}^2\left\{\frac{1}{2}\sqrt{\frac{3a}{h_0^2(h_0+a)}}\left[x-\sqrt{\boldsymbol{g}(h_0+a)}\,t\right]\right\} \quad (18)$$

Here, ζ refers to the free surface above still water level; a is amplitude, h_0 is still the water depth, $\boldsymbol{g}$ is the gravitational acceleration, and t is the time. Reference [10] also derives the following expression for horizontal velocity components in the positive x-direction:

$$u(x,y,t) = c\left(1-\frac{h_0}{\zeta(x,y,t)+h_0}\right)\ ,\ v(x,y,t) = 0 \quad (19)$$

For oblique solitary wave, the coordinate axis is transformed. Hence, the horizontal velocity components are

$$\begin{aligned} u(x',y',t) &= c\left(1-\frac{h_0}{\zeta(x',y',t)+h_0}\right).\cos(\theta) \\ v(x',y',t) &= c\left(1-\frac{h_0}{\zeta(x',y',t)+h_0}\right).\sin(\theta) \end{aligned} \quad (20)$$

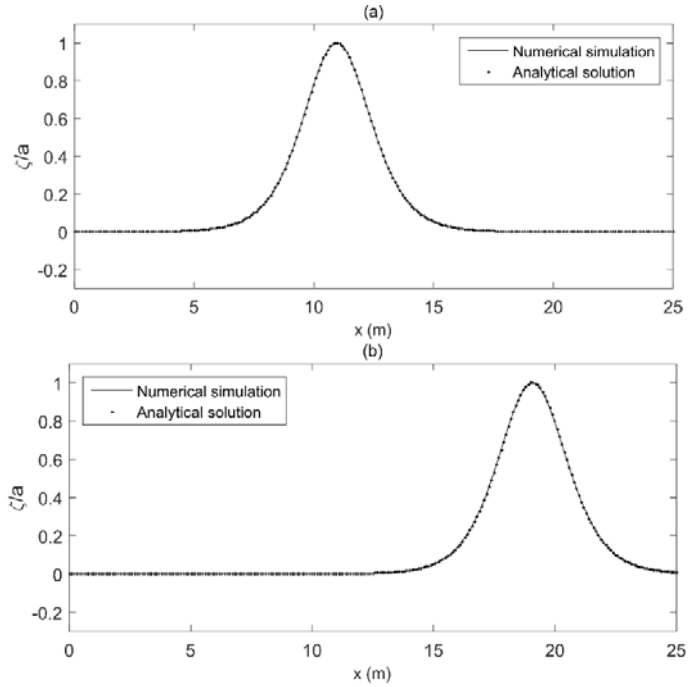


Fig. 5 Comparison between numerical prediction (solid line) and analytical solution (cross symbols) of free surface elevation profiles of solitary wave at times (a) t = 1 s and (b) t = 3 s

Open Science Index, Aerospace and Mechanical Engineering Vol:12, No:3, 2018 publications.waset.org/10008925/pdf

Open Science Index, Aerospace and Mechanical Engineering Vol:12, No:3, 2018 publications.waset.org/10008925/pdf

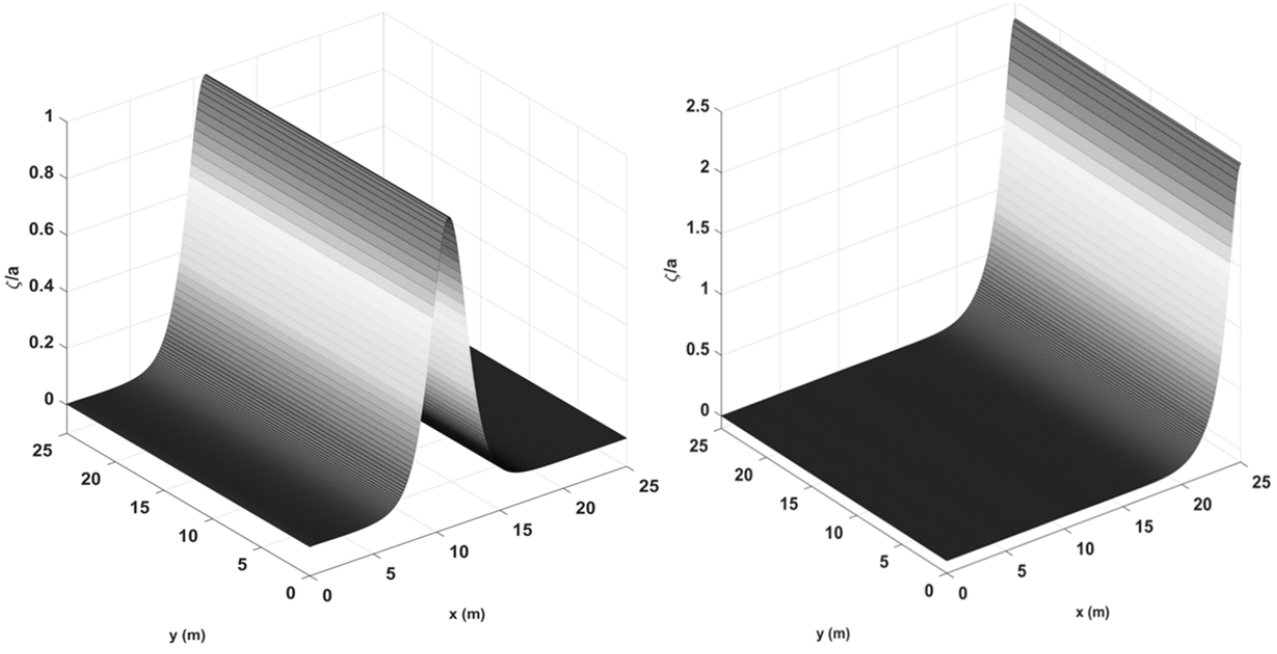
where

$$x' = x\cos(\theta) - y\sin(\theta)$$
$$y' = x\sin(\theta) + y\cos(\theta) \quad (21)$$

x' and y' are the transformed coordinate axis. A basin of 25 m length and 25 m width is selected. The still water depth is h_0 = 1 m and the solitary wave has amplitude of a = 0.6 m. Two solitary wave tests were undertaken; one where the wave propagates from west to east in the positive x-direction, and another where the wave propagates at an angle θ = 30° to the x-axis. Figs. 5 (a) and (b), respectively, show direct comparison between numerical prediction and analytical solution of the free surface profiles of solitary wave at times t = 1 s and 3 s where the wave propagates from west to east in the positive x-direction. Figs. 5 (a) and (b) represent complete agreement between the numerical prediction and the linear analytical solution. This case verifies that the numerical scheme yields a correct representation of the underlying mathematical description provided that the waves are nearly linear. Figs. 6 (a)-(c) depict 3D visualisation of the numerical predictions of evolution of the solitary wave at times t = 1, 5, and 10 s on the converged grid with $\Delta x = \Delta y$ = 100 mm and time step Δt = 0.05 s where the wave propagates from west to east in the positive x-direction over flat-bed basin. At first, the solitary wave propagates with its free surface profile unchanging in shape as it moves along the channel (see result at t = 1 s). At t ~ 5 s, the solitary wave crest hits the wall and its elevation, runs up elevation, reaches 2.355 m which is more than twice the elevation prior to contact. The reflected wave sheds some trailing waves which are evident behind the reflected wave as it travels from east to west as shown in the plot for t = 10 s. Comparison between the present GN numerical solver prediction and result from perturbation analysis confirms that nonlinear interaction between a solitary wave and a solid wall is correctly modelled. Based on perturbation analysis, the total run up elevation, R, is:

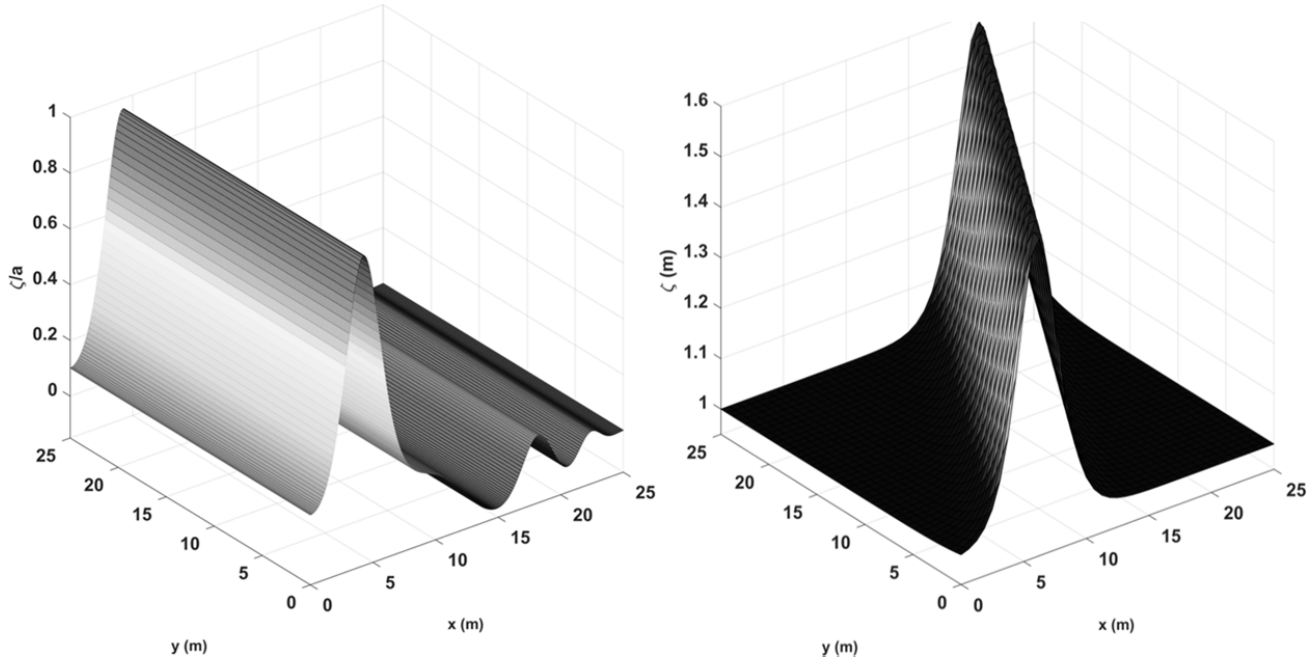
$$R = h_0\left\{1 + 2s + \frac{s^2}{2} - \frac{s^3}{4} + \frac{s^4}{4} - \frac{s^5}{4} + \frac{7s^6}{32} - \frac{9s^7}{64} + \frac{s^8}{128} + O[s]^9\right\} \quad (22)$$

in which s is amplitude of wave (a) divided by still water depth (h_0). By including the second-order perturbation term, the approximated analytical solution for the reflected solitary wave elevation is 2.3454 m, a quite similar value to that predicted by the GN model (2.355 m). The next verification test of 2D level I GN equations comprises the simulation of an oblique solitary wave (θ = 30°) in a 25 m by 25 m basin. Fig. 6 (d) depicts the numerical solver visualisation of free surface profile at t = 0.1 s. The oblique wave retains its shape with time as it moves from west to east, except at the boundaries where wall interactions take place. This indicates that the model can cope properly with a wave at an angle to the grid.



(a) (b)

Open Science Index, Aerospace and Mechanical Engineering Vol:12, No:3, 2018 publications.waset.org/10008925/pdf



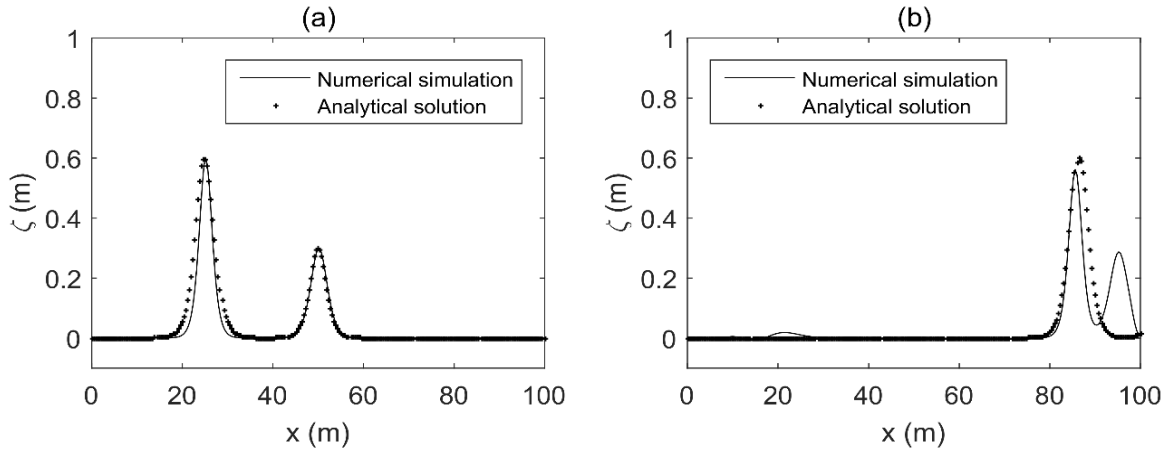
(c) (d)

Fig. 6 Numerically predicted 3D visualisation of free surface profiles of solitary wave: The solitary wave moving west to east in positive x-direction at (a) t = 1 s, (b) t = 5 s, (c) t = 10 s, and (d) oblique solitary wave profile (θ = 30°) at t = 0.1 s

VIII. Interaction of Two Solitary Waves in Wall-Bounded Basin

Solitary waves of 0.6 m and 0.3 m initial amplitudes in otherwise still water of depth 1 m are simulated in a closed basin of planned dimensions $L_x = L_y = 100$ m. The convergence predictions for numerical scheme are obtained on fine grids $\Delta x = \Delta y = 100$ mm and a fixed time step $\Delta t = 0.05$ s. Fig. 7 presents evolution of the two solitary waves at (a) $t = 0$ s, (b) $t \sim 16$ s, (c) $t = 17$ s, and (d) $t \sim 18$ s where the waves propagate from west to east in the positive x-direction. In Fig. 7, free surface profiles of the solitary waves are simulated by linear analytical solution (cross symbols) and numerical solver (solid line).

In numerical prediction at $t \sim 16$ s, the large-amplitude solitary wave reaches the small-amplitude solitary wave, and after the collision of small-amplitude wave with the wall, the two waves will be merged at $t = 17$ s. The elevation of the combined wave reaches 0.932 m in numerical prediction. The elevation of the combined wave in analytical prediction is 0.6 m which is equal to the amplitude of the large wave. The foregoing discrepancies are largely due to nonlinear wave interaction modelled by the GN equations. Finally, at $t \sim 18$ s, numerical waves with different amplitudes propagate separately.



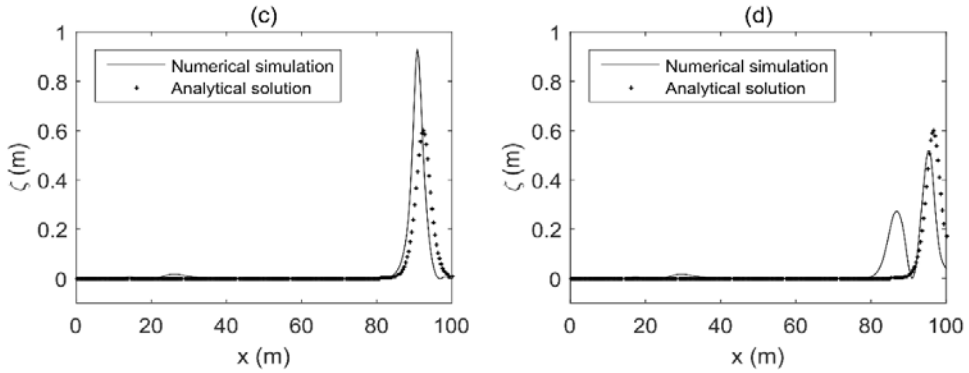


Fig. 7 Comparison between analytically predicted free surface elevation profile (cross symbols) and numerically predicted free surface elevation profile (solid line) for the interaction of two solitary waves at (a) $t = 0$ s; (b) $t \sim 16$ s; (c) $t = 17$ s; and (d) $t \sim 18$ s

Open Science Index, Aerospace and Mechanical Engineering Vol:12, No:3, 2018 publications.waset.org/10008925/pdf

IX. Conclusion

This study presents the 2D level I GN equations and their discretisations using second-order finite differences in space and a fourth-order Runge-Kutta scheme in time. To verify the developed numerical solver of 2D GN equations, a series of standard benchmark tests were performed including free surface sloshing of even harmonic components of an initial Gaussian hump and solitary wave propagation. The analytical solution was not capable of showing the nonlinear behaviour of even harmonics. However, the effect of nonlinearity was evident in numerical predictions of the even harmonics. The even harmonics had amplitudes of up to about 20% that of the initial hump. FFT analyses were also performed to highlight the frequency content of the results. All five peaks of numerical even harmonics occurred at the same frequency of the analytically predicted peaks of Gaussian hump. It was observed that numerical solver produced accurate simulations of solitary wave propagation when the results were compared against a standard linear solution. Comparison between the numerical prediction and result obtained from perturbation analysis confirmed that nonlinear interaction between solitary wave and a solid wall was correctly modelled. When the solitary wave hits the wall, the numerically predicted run up reaches 2.355 m which is 0.355 m more than the predicted linear analytical solution. By including the second-order perturbation term, the approximated analytical solution for the reflected solitary wave elevation was 2.3454 m, a quite similar value to the run up elevation predicted by the GN model. Simulation of solitary wave propagated at an angle $\theta = 30^{o}$ to the x-axis showed that the model was capable of coping with a wave at an angle to the grid. The developed GN numerical solver produced accurate predictions of interaction of two solitary waves. The discrepancies between numerical simulation and analytical solution were largely due to nonlinear wave interactions which are adequately modelled by the developed GN equations. However, the nonlinearity of wave interactions is completely neglected in the analytical solution.

References

[1] R. A. Ibrahim, *Liquid sloshing dynamics theory and applications*. Cambridge, Cambridge University Press, 2005, Introduction.

[2] M. R. Jalali, *One-Dimensional and Two-Dimensional Green-Naghdi Equation Solvers for Shallow Flow over Uniform and Non-Uniform Beds*. Edinburgh, The University of the Edinburgh, 2016, pp. 20–67.

[3] R. H. Stewart, *Introduction to Physical Oceanography*. Texas, Texas A & M University, 2008, pp. 273–280.

[4] A. E. Green and P. M. Naghdi. ''Directed Fluid Sheets'', *Proc. of the Royal Society of London. Series A, Mathematical and Physical Sciences J.*, vol. 347, no. 1651, pp. 447–473, 1976.

[5] W. C. Webster and J. J. Shields, ''Applications of high-level Green-Naghdi theory to fluid flow problems'', W. G. Price, P. Temarel, and A. J. Keane, Eds, *In Dynamics of Marine Vehicles and Structures in Waves*, *Elsevier Science*, Amsterdam, 1991.

[6] Z. Demirbilek and W. C. Webster, *Application of the Green-Naghdi theory of fluid sheets to shallow-water wave problems*, *Report 1*, *Model Development*. US Army Engineers Waterways Experiment Station, Coastal Engineering Research Center, DC, Technical Report CERC–92–11, 1992.

[7] R. C. Ertekin, (1984) *Soliton Generation by Moving Disturbances in Shallow Water: Theory, Computation and Experiment*. California, University of California, 1984.

[8] J. J. Shields and W. C. Webster. ''On direct methods in water-wave theory''. *Fluid Mechanics J.*, vol. 197: pp. 171–199, 1988.

[9] J. W. Kim and R. C. Ertekin, ''A numerical study of nonlinear wave interaction in regular and irregular seas: irrotational Green-Naghdi model''. *Marine Structures J.*, vol. 13, no. 45, pp. 331–347, 2000.

[10] O. Le Métayer, S. Gavrilyuk, and S. Hank. ''A numerical scheme for the Green-Naghdi model'', *Computational Physics J.*, vol. 229, no. 6, pp. 2034–2045, 2010.

[11] M. Hayatdavoodi and R. C. Ertekin. ''Wave forces on a submerged horizontal plate. Part II: Solitary and cnoidal waves''. *Fluids and Structures J.*, vol. 54: pp. 580–596, April 2015.

[12] R. C. Ertekin, M. Hayatdavoodi, and J. W. Kim, ''On some solitary and cnoidal wave diffraction solutions of the Green-Naghdi equations''. *Applied Ocean Research J.*, vol. 47: pp. 125–137, August 2014.

[13] B. B. Zhao, R. C. Ertekin, W. Y. Duan and M. Hayatdavoodi, (2014) ''On the steady solitary-wave solution of the Green-Naghdi equations of different levels''. *Wave Motion J.*, vol. 51, no. 8, pp. 1382–1395, 2014.

[14] M. R. M. Haniffah, *Wave Evolution on Gentle Slopes-Statistical Analysis and Green-Naghdi Modelling*. Oxford, University of Oxford, 2013, pp. 73–92.

[15] M. R. Jalali and A. G. L Borthwick, ''One-dimensional and two-dimensional Green–Naghdi equations for sloshing in shallow basins'', *Proc. Of the Inst. of Civil Engineers-Engineering and Computational Mechanics*, vol. 170, no. 2: pp. 49–70, 2017.

[16] W. H. Press, S. A. Teukolsky, W. T. Vetterling, and B. P. Flannery, *Numerical recipes the art of scientific computing. Solution of linear algebraic equations*. Cambridge, Cambridge University Press, 2007.

[17] T. Johannessen and C. Swan. ''A laboratory study of the focusing of transient and directionally spread surface water waves''. *Proc. of the Royal Society of London. Series A, Mathematical, Physical and Engineering Sciences*, vol. 457, no. 2008, pp. 971–1006, 2001.

[18] A. C. Hunt, P. H. Taylor, A. G. L. Borthwick, and P.K. Stansby. ''Phase inversion and the identification of harmonic structure in coastal engineering experiments''. *in Pro. 29th Int. Conf. on Coastal Engineering*, Lisbon, 2004, pp. 1047–1059.